Infrared study of the quasi-two-dimensional electron system at the interface between SrTiO3 and crystalline or amorphous LaAlO3

Infrared study of the quasi-two-dimensional electron system at the interface between $SrTiO_3$ and crystalline or amorphous $LaAlO_3$

A. Nucara,[1] M. Corasaniti,[2] A. Kalaboukhov,[3] M. Ortolani,[2] E. Falsetti,[2] A. Sambri,[4] F. Miletto Granozio,[4] F. Capitani,[5] J.-B. Brubach,[5] P. Roy,[5] U. Schade,[6] and P. Calvani[1]

[1]*CNR-SPIN and Dipartimento di Fisica, Università di Roma "La Sapienza," Piazzale A. Moro 2, I-00185 Rome, Italy*
[2]*Dipartimento di Fisica, Università di Roma "La Sapienza," Piazzale A. Moro 2, I-00185 Rome, Italy*
[3]*Department of Microtechnology and Nanoscience, Chalmers University, S-41296 Gothenburg, Sweden*
[4]*CNR-SPIN UOS Napoli, Complesso Universitario di Monte Sant'Angelo, Via Cinthia, I-80126 Naples, Italy*
[5]*Synchrotron SOLEIL, L'Orme des Merisiers Saint-Aubin, Boîte Postale 48, F-91192 Gif-sur-Yvette Cedex, France*
[6]*Methoden der Materialentwicklung, Helmholtz-Zentrum Berlin für Materialien und Energie GmbH, D-12489 Berlin, Germany*

(Received 6 October 2017; revised manuscript received 20 February 2018; published 13 April 2018)

We have used grazing-angle infrared spectroscopy to detect the Berreman effect (BE) in the quasi-two-dimensional electron system (q-2DES) which forms spontaneously at the interface between $SrTiO_3$ (STO) and a thin film of $LaAlO_3$ (LAO). From the BE, which allows one to study longitudinal optical excitations in ultrathin films like the q-2DES, we have extracted at different temperatures its thickness, the charge density and mobility of the carriers under crystalline LAO (sample A), and the charge density under amorphous LAO (sample B). The latter quantity turns out to be higher than in sample A, but a comparison with Hall measurements shows that under amorphous LAO the charges are partly localized at low T with a low activation energy (about 190 K in units of k_B) and are thermally activated according to a model for large polarons. The thickness of the q-2DES extracted from our spectra turns out to be 4 ± 1 nm for crystalline LAO and 7 ± 2 nm for amorphous LAO.

DOI: 10.1103/PhysRevB.97.155126

I. INTRODUCTION

The interest in two-dimensional electron systems (2DESs) dates back at least to the observation of Wigner electron crystals on the surface of superfluid helium [1]. However, studies on 2DESs have reached their widest diffusion in solid-state physics, through the fabrication of semiconductor-based heterostructures for the implementation of electronic and photonic devices. In the last decade, moreover, it has been discovered that a 2DES may form spontaneously in systems of extraordinary interest like graphene [2], topological insulators [3,4], and the interfaces between insulating oxides. The most-studied 2DES in oxides is the free-electron layer which forms within the upper TiO_2 layer of a $SrTiO_3$ (STO) substrate, when a $LaAlO_3$ (LAO) film thicker than four unit cells [5,6] is deposited on it. The thickness of this electron layer is not larger than 10 nm [7,8], and for this reason it is often called a quasi-2DES (q-2DES). Among the intriguing properties of the LAO/STO q-2DES, both ferromagnetism at low temperatures [9] and superconductivity below 200 mK [10] have been reported, two phenomena which can also coexist [11,12]. Similar two-dimensional electron systems have been also observed in $NdGaO_3/SrTiO_3$ [13] and $LaAlO_3/EuTiO_3/SrTiO_3$ [14].

The q-2DES formation is basically explained in terms of a top-down charge transfer aimed at preventing a "polar catastrophe" within LAO [5,15]. Nevertheless, several authors have stressed the role of the oxygen vacancies [16,17] which may form during the film's growth, survive to the standard annealing procedures, and dope the interface with electrons. The latter mechanism may better explain why a 2DES similar to that of crystalline LAO is also observed under amorphous LAO [18]. While the dc conducting properties of the 2DES in LAO/STO have been determined since the beginning [19], to our knowledge only a couple of experiments have been devoted to studying its low-energy electrodynamics [8,20]. In fact, determining the frequency-dependent response of ultrathin metallic films is a challenging task for conventional infrared spectroscopy. Both the above-cited experiments indeed obtained reliable results by exploiting an important effect discovered by Berreman in 1963 [21].

In the Berreman effect (BE), the p component of the electric field (in the plane of incidence) undergoes enhanced absorption through a film of thickness d if d is much smaller than both the radiation wavelength λ and the field penetration depth d_p. The BE thus allows one to investigate the low-energy electrodynamics of very thin films. However, it occurs only at frequencies ω close to that where the real part of the film dielectric function $\epsilon_1(\omega)$ vanishes. Consider, for sake of simplicity, a film (index f) self-supporting in a vacuum (index 0). If the angle of incidence θ is large, the p-polarized component of the incident electric field is strong and enters the film normal to its surface [$E_n^0(\omega)$]. Therein, it becomes $E_n^f(\omega) = D_n^f(\omega)/\epsilon_1(\omega)$, where $\epsilon_1(\omega)$ is the real part of the dielectric function and $D_n^f(\omega)$ is the normal component of the electric displacement field. As $D_n^f = D_n^0 = E_n^0$ for the continuity equations, at ω's such that $\epsilon_1(\omega) \simeq 0$, one has both a pole in the energy loss function and a strong field enhancement [$E_n^f(\omega) \gg E_n^0(\omega)$]. Thus, in a film thinner than both λ and d_p, $E_n(\omega)$ creates a dynamical dipole moment which resonates with the longitudinal excitations of the sample [22]. The same mechanism works in thin films deposited on a substrate, provided that suitable formulas (see

Sec. III) are used to take into account the optical response of the various interfaces. The excitations detectable in a BE experiment include the vibrations of a thin layer of adsorbed molecules, the longitudinal optical phonons of insulating thin films (at frequencies ω_L), and the screened plasma frequency $\omega_p/\sqrt{\epsilon_\infty}$ of metallic films (where ϵ_∞ is the real part of the dielectric function for $\omega \gg \omega_p$).

The object of the present investigation is indeed the response to grazing-angle incident radiation of the few-nanometer-thick q-2DES at the interface between $LaAlO_3$ (either crystalline or amorphous) and $SrTiO_3$. Unlike in previous similar experiments [8,20], we did not use a real ellipsometric apparatus, but we measured at the grazing angle by using a single polarizer and synchrotron radiation the ratio R_p/R_s, where R_p and R_s are the LAO/STO reflectances in p and s polarizations, respectively. Afterwards, in order to compare our results with those in the literature, we determined the ellipsometric angle

$$\Psi(\omega) = \arctan(R_p/R_s)^{1/2} = \arctan[|\tilde{r}^p(\omega)|/|\tilde{r}^s(\omega)|], \quad (1)$$

where $\tilde{r}^p$ and $\tilde{r}^s$ are the complex reflection coefficients in the two polarizations [23]. In order to measure R_p/R_s one just has to remotely turn a polarizer in front of the sample and then to repeat the same operation after shifting the mirror to the sample position without acting on the optics or on the sample. Moreover, in order to check that the observed BE comes from the q-2DES, we measured $\Psi(\omega)$ in a third LAO/STO sample, where the q-2DES was erased by ion etching [24], that was used as reference. This will allow us to extract the predicted shape of the Berreman resonance [8], which consists of a dip-peak feature in the difference between the angles Ψ measured in the sample with the q-2DES and in the no-q-2DES reference. By fitting the optical formulas reported in Sec. III to the data we can then determine the electrodynamic parameters of the q-2DES for both crystalline and amorphous LAO. In the former case we substantially confirm the results of Ref. [8] using a somewhat simpler procedure, while the present measurements on amorphous LAO are unique. They show a q-2DES charge density remarkably higher than under crystalline LAO, but a comparison with Hall measurements shows that the charges are partly localized at low T with a low activation energy (190 K in units of k_B), suggesting that they may form large polarons.

II. EXPERIMENT AND RESULTS

Two crystalline LAO films (samples A and C) and an amorphous-LAO film (sample B) were deposited on TiO_2-terminated $SrTiO_3$ substrates by pulsed laser deposition. In samples A and C, LAO was ten unit cells (4 nm) thick, so that it could develop the 2DES at the interface with STO while its absorption was negligible [8,24]. The samples were grown [25] at a substrate temperature of 800 °C and under an oxygen pressure of 10^{-4} mbar, then further annealed for 1 h at 600 °C and 500 mbar. The sheet resistance of the conducting q-2DES at the interface was reported in Ref. [24]. Sample B was grown at room temperature by pulsed laser deposition using a KrF excimer laser at an oxygen pressure of 5×10^{-4} mbar. The LAO thickness was 5 nm based on calibrations made on the reflection high-energy electron diffraction oscillations of a twin crystalline sample grown at room temperature. The sheet resistance of sample B is reported in Fig. 6 below.

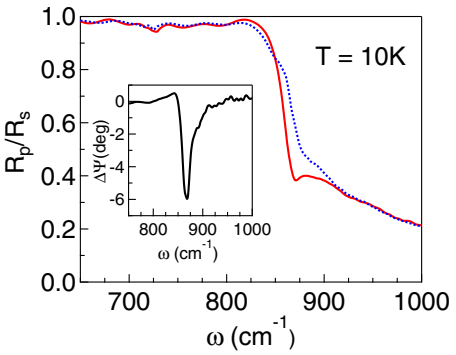

FIG. 1. Ratio R_p/R_s measured at the IRIS beamline of BESSY II in the amorphous-LAO/STO sample (sample B) with the q-2DES (solid red line) and in the LAO/STO sample (C) without the q-2DES (dotted blue line) at 10 K. The inset shows the difference $\Delta\Psi = \Psi_B - \Psi_C$ between the ellipsometric angles calculated with Eq. (1) for samples B and C. The profound dip at 868 cm^{-1} is caused by the Berreman effect in the q-2DES.

Afterwards, the q-2DES in sample C was erased by ion milling dry etching as described in Ref. [25], where the procedure was shown to damage LAO/STO within a depth of just 1 nm. The low-energy ion irradiation does not etch the LAO film, and the morphological and chemical properties of sample C are very similar to those of sample A, but without a conducting layer. Sample C was measured in the same way as samples A and B to be used as a reference.

The reflectivity $R_j(\omega)$ of samples A, B, and C was measured in both polarizations $j = p,s$ under an angle of incidence $\theta = 72°$ by Michelson interferometers and mercury cadmium telluride detectors cooled by liquid nitrogen. In order to improve the signal-to-noise ratio at grazing incidence, we have exploited the higher brilliance of infrared synchrotron radiation with respect to conventional black bodies [26]. Preliminary measurements at the IRIS beamline of BESSY II were repeated and completed at the AILES beamline of SOLEIL using a different apparatus. In both experiments the samples were thermoregulated within ±2 K. Golden mirrors placed above the sample and aligned parallel to it by a laser beam were used as references. An external mechanism allowed us to illuminate either the sample or the mirror. A single KRS-5 polarizer having a contrast better than 99.9% that could be remotely rotated was put on the radiation path. The optics of the interferometer confined the energy of the incident radiation below 1.5 eV, namely, below both the STO gap (3.2 eV) and the subband gap levels reported in Ref. [27]. This prevented any possible photodoping of the interface. At each temperature, two 300-scan series of interferograms were taken on the sample, in both p and s polarizations, with a spectral resolution of 2 cm^{-1}. The same sequence was then repeated at each temperature for the Au mirror. We thus obtained the reflectances R_p and R_s shown in Fig. 2 of the Supplemental Material (SM) [28] and, using Eq. (1), the ellipsometric angle $\Psi(\omega)$ for samples A, B, and C.

The ratios R_p/R_s measured at BESSY II in sample B, which has the q-2DES, and in sample C, where the q-2DES had been erased, are shown in Fig. 1 at 10 K in the region of the hardest longitudinal phonon of STO (L3). A strong anomaly appears above its frequency $\omega_{L3} = 790$ cm^{-1} only in

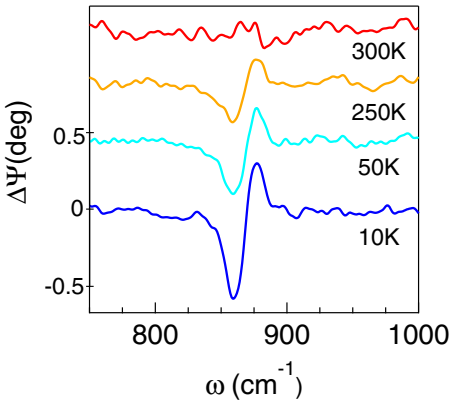

FIG. 2. Berreman effect caused by the q-2DES at the interface between crystalline LAO and STO, as obtained by subtracting from $\Psi(\omega)$ of sample A that measured in LAO/STO without the q-2DES (sample C). The vertical scale reported for $T = 10$ K holds also for the other temperatures where the zeros have been shifted for clarity. Data were taken at the AILES beamline of SOLEIL.

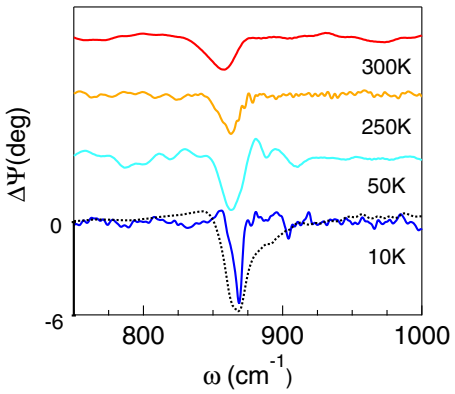

FIG. 3. Berreman effect caused by the q-2DES at the interface between amorphous LAO and STO, as obtained by subtracting from $\Psi(\omega)$ of sample B that measured in LAO/STO without q-2DES (sample C). The vertical scale reported for $T = 10$ K holds also for the other temperatures, where the zeros have been shifted for clarity. Data were taken at the AILES beamline of SOLEIL. The corresponding data obtained at BESSY II at 10 K on the same sample but with a different optical setup are reported for comparison by a dashed line on the same scale (see text).

the former spectrum. This comparison shows that the anomaly is fully associated with the q-2DES and that sample C, quite similar to the other ones except for the first nanometer-thick layer from the surface, can be used as reference in a sort of differential spectroscopy. The inset shows the difference $\Delta\Psi = \Psi_B - \Psi_C$ between the ellipsometric angles calculated using Eq. (1) for samples B and C. A similar procedure was used in Ref. [8], where, however, the reference was a bare STO substrate. The resulting dip at 868 cm^{-1}, about 80 cm^{-1} from ω_{L3}, is characteristic of the Berreman effect and can be entirely ascribed to the q-2DES. Such a dip is much stronger than that observed previously [8,20] and also in the present experiment (see below) under crystalline LAO.

Figure 2 shows the results of the same experiment when applied to crystalline LAO on STO (sample A) at different temperatures. In $\Delta\Psi = \Psi_A - \Psi_C$, a full Berreman resonance is observed, consisting of a dip at 859 cm^{-1} followed by a peak at $\omega_{Ber} = 875$ cm^{-1}, as observed in Ref. [8] for crystalline LAO/STO. The peak is shifted by about 85 cm^{-1} from the ω_{L3} of STO. The fact that ω_{Ber} is independent of temperature is consistent with both the prediction that the peak frequency is determined essentially by the carrier density in the q-2DES [8,20] and the fact that this latter has a really metallic behavior in the infrared.

Figure 3 displays instead $\Delta\Psi = \Psi_B - \Psi_C$ for the q-2DES under amorphous LAO at different temperatures, as obtained from data collected at SOLEIL. At 10 K, those taken at BESSY II are shown again for comparison by the dotted line. All spectra in Fig. 3 show a Berreman dip much more pronounced than in Fig. 2, while the Berreman peak at ω_{Ber} is not observed. This point will be discussed in the next section. The $\Delta\Psi$ obtained at 10 K with the two different apparatuses provide a Berreman dip at the same frequency and with the same amplitude within error. However, the BESSY II source provides, on the one hand, a better signal-to-noise ratio and, on the other hand, a larger dip linewidth. As it results from the calculations of Ref. [29], the dip width has no particular meaning because it is not related to the carrier relaxation time, which instead affects the Berreman peak. Here, we attribute the width mismatch between the two apparatuses to the helium-flow cryostat windows, which at BESSY II may slightly mix the p and s components after the polarizer. At SOLEIL there are no such windows, as the sample is cooled by a cryogenerator and the whole optical chamber, including the polarizer, is in a high vacuum.

III. DATA ANALYSIS AND DISCUSSION

The analysis of the spectra proceeded as follows. We assume that the 4-nm-thick LAO is transparent at all frequencies and that the STO substrate with thickness $d = 0.5$ mm is a semi-infinite medium. The latter hypothesis has been checked by fitting the reflectivity of the no-2DES sample (sample C) with d as a free parameter. We then modeled the samples with the q-2DES by an optical double layer [30] formed by a conducting STO film of thickness d and refraction index $\tilde{n}_1$, which contains the free charges, and by the STO substrate of index $\tilde{n}_2$. Two interfaces of the q-2DES are both transmitting and reflecting, the one with a vacuum (indexed as 01) and the one with the insulating STO (indexed as 12). One then has for the reflection coefficients of the entire multilayer [31]

$$\tilde{r}^j_{012} = \frac{\tilde{r}^j_{01} + \tilde{r}^j_{12}\exp(2i\delta)}{1 + \tilde{r}^j_{01}\tilde{r}^j_{12}\exp(2i\delta)}, \tag{2}$$

where $j = p,s$ identifies the polarization, $\delta = 2\pi\tilde{n}_1 d/\lambda_0$, and λ_0 is the radiation wavelength in a vacuum. For sample C, $r^j_{12} = 0$, and the reflectivity reduces to that of bulk STO.

In Eq. (2), the reflection coefficients at the interface with a vacuum ($\tilde{n}_0 = 1$) for an angle of incidence θ (here 72°) are given by the Fresnel formulas [31],

$$\tilde{r}^p_{01} = \frac{\tilde{n}^2\cos\theta - \sqrt{\tilde{n}^2 - \sin^2\theta}}{\tilde{n}^2\cos\theta + \sqrt{\tilde{n}^2 - \sin^2\theta}},$$
$$\tilde{r}^s_{01} = \frac{\cos\theta - \sqrt{\tilde{n}^2 - \sin^2\theta}}{\cos\theta + \sqrt{\tilde{n}^2 - \sin^2\theta}}, \tag{3}$$

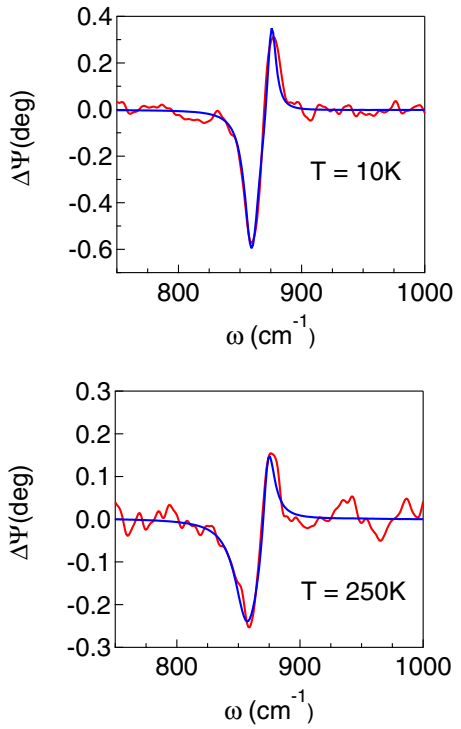

FIG. 4. Fits at two temperatures using Eqs. (1) to (6) (blue lines) to the experimental $\Delta\Psi = \Psi_A - \Psi_C$ in Fig. 2 (red lines) for crystalline LAO on STO.

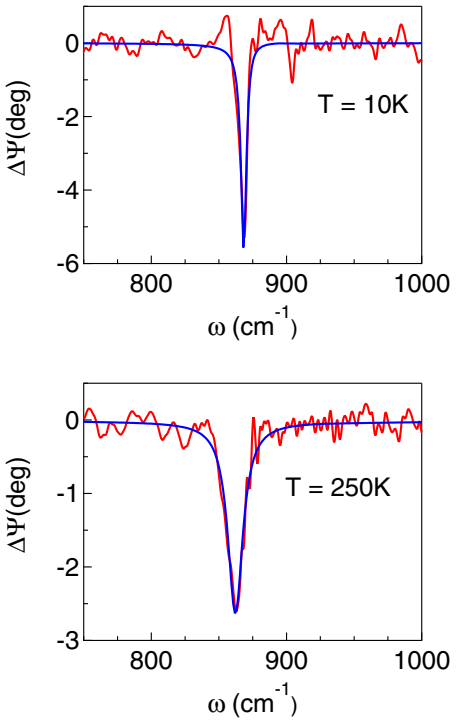

FIG. 5. Experimental $\Delta\Psi = \Psi_B - \Psi_C$ (red lines) from data taken at the AILES beamline of SOLEIL, showing the Berreman effect in amorphous LAO on STO at two temperatures. The blue lines are the fits to data obtained from Eqs. (1) to (6).

where $\tilde{n} = \tilde{n}_1$ for the conducting samples A and B and $\tilde{n} = \tilde{n}_2$ for the insulating STO sample C. In turn, the reflection coefficients at the interface between conducting and insulating STO are obtained with

$$\tilde{r}_{12}^{p} = \frac{(\tilde{n}_2/\tilde{n}_1)^2 \cos\theta - \sqrt{(\tilde{n}_2/\tilde{n}_1)^2 - \sin^2\theta}}{(\tilde{n}_2/\tilde{n}_1)^2 \cos\theta + \sqrt{(\tilde{n}_2/\tilde{n}_1)^2 - \sin^2\theta}},$$
$$\tilde{r}_{12}^{s} = \frac{\cos\theta - \sqrt{(\tilde{n}_2/\tilde{n}_1)^2 - \sin^2\theta}}{\cos\theta + \sqrt{(\tilde{n}_2/\tilde{n}_1)^2 - \sin^2\theta}}. \quad (4)$$

The refraction index for the no-2DES sample, $\tilde{n}_2 = \sqrt{\tilde{\epsilon}_2}$, is obtained with the Lyddane-Sachs-Teller expression for the complex dielectric function for STO [32],

$$\tilde{\epsilon}_2(\omega) = \epsilon_\infty \prod_j \frac{(\Omega_{Lj}^2) - \omega^2 + i(\Gamma_{Lj})\omega}{(\Omega_{Tj}^2) - \omega^2 + i(\Gamma_{Tj})\omega}, \quad (5)$$

where Ω_j and Γ_j are the central frequency and width, respectively, of the jth longitudinal (L) or transverse (T) optical phonon. In turn, the refraction index in the presence of the q-2DES $\tilde{n}_1 = \sqrt{\tilde{\epsilon}_1}$ is calculated by adding to Eq. (5) a free-electron Drude term, so that

$$\tilde{\epsilon}_1(\omega) = \tilde{\epsilon}_2(\omega) + \tilde{\epsilon}_D(\omega) = \tilde{\epsilon}_2(\omega) - \frac{\omega_p^2}{\omega^2 + i\omega\Gamma_D}. \quad (6)$$

The curves obtained by fitting to data equations (1) to (6) are shown at different temperatures in Figs. 4 and 5 for crystalline and amorphous LAO, respectively. Despite the numerous equations involved and the weakness of the Berreman effect in the q-2DES, the fits are quite satisfactory. The resulting parameters of the Drude-Lorentz model for the conducting film are reported in Table I. The other phonon frequencies and widths were fixed to the values reported in Table II of Ref. [24]. The q-2DES thickness is independent of temperature within errors and turns out to be 4 ± 1 nm under crystalline LAO, consistent with the direct determination of Ref. [7] ($d < 7$ nm), but increases to 7 ± 2 nm under amorphous LAO.

The quantities which describe the conducting properties of the q-2DES, as obtained from the fitting parameters in Table I, are reported in Table II. Therein, the electron surface density is $n_s^{IR} = n^{IR}d = dm^*\epsilon_0\omega_p^2/e^2$ (where [8] $m^* = 3.2m_e$ and m_e is the bare-electron mass). Both values turn out to be much lower under crystalline LAO (sample A) than under amorphous LAO (sample B). In sample A, n_s is also lower than that measured

TABLE I. Fitting parameters for the q-2DES at the interface between crystalline (sample A) or amorphous (sample B) LAO and STO. The plasma frequency ω_p, the relaxation rate Γ_D, the highest LO-phonon frequency, and width for STO are all expressed in cm^{-1}. For the parameters of the other STO phonons we used the values in Table II of Ref. [24]. The observation of the dip alone does not allow us [29] to give a meaningful determination of Γ_D in sample B.

Sample (T)	d (nm)	ω_p	Γ_D	ω_{L3}	Γ_{L3}
A (250 K)	4 ± 1	980 ± 80	155 ± 20	784	35
A (10 K)	4 ± 1	950 ± 80	5 ± 2	784	23
B (250 K)	7 ± 2	3000 ± 500		787	27
B (10 K)	7 ± 2	2900 ± 500		794	16

TABLE II. Surface density n_s^{IR} and bulk density n^{IR} of the q-2DES carriers at the interface between STO and crystalline (A) or amorphous (B) LAO at two temperatures, as extracted from the parameters of Table I with $m^* = 3.2m_e$ [8]. The carrier mobility μ^{IR} is extracted from the Berreman peak width Γ_D (observed only in sample A). The dc mobility μ^{dc} is extracted from the data in Ref. [24] for sample A and from Fig. 6 in the main text and Fig. 1 of the Supplemental Material [28] for sample B.

Sample (T)	n_s^{IR} (cm^{-2})	n^{IR} (cm^{-3})	μ^{IR} (cm^2/V s)	μ^{dc} (cm^2/V s)
A (250 K)	$(1.4 \pm 0.3) \times 10^{13}$	$(3.4 \pm 0.2) \times 10^{19}$	20 ± 2	8 ± 1
A (10 K)	$(1.3 \pm 0.3) \times 10^{13}$	$(3.2 \pm 0.2) \times 10^{19}$	580 ± 40	560 ± 30
B (250 K)	$(2.3 \pm 0.7) \times 10^{14}$	$(3.2 \pm 0.3) \times 10^{20}$		10 ± 2
B (10 K)	$(2.2 \pm 0.7) \times 10^{14}$	$(3.0 \pm 0.3) \times 10^{20}$		2200 ± 200

in the carrier-richest sample of Ref. [8] but comparable with that reported for another sample in the same experiment. For sample A at both temperatures (10 and 250 K), the carrier mobility $\mu^{IR} = e/(2\pi m^* c\Gamma)$ is in very good agreement with the dc mobility μ^{dc}, also reported for comparison in Table II. It was extracted from the dc measurements of Ref. [24] and from the present n_s^{IR}.

In order to better understand the behavior of sample B, we also performed dc transport and Hall measurements on it aimed at determining its electrodynamic properties vs temperature at zero frequency. The results are shown in Fig. 6. In the inset, n_s^{dc} is roughly constant between 300 and 100 K, decreasing by a factor of 3 between about 100 and 10 K. Such a decrease is not observed in our midinfrared spectra, and similar discrepancies were reported in Fig. 2 of Ref. [8] for LAO/STO, in Ref. [20] again for LAO/STO, and in Ref. [33] for γ-Al_2O_3/STO. Therein, the disagreement was explained in terms of polaronic effects [34]. Indeed, the mobility values in Table II are consistent, e.g., with polaronic transport in TiO_2 [35]. The weak localization observed in the q-2DES below 100 K in the inset of Fig. 6 for amorphous LAO and in Fig. 2 of Ref. [8] for crystalline LAO points to polarons of the "large" type [36]. As usual, one can assume for the variable-temperature dependence of $n_s(T)$ an Arrhenius law [37] with a binding energy Δ. Moreover, under the assumption of scattering by acoustic phonons at not too high temperatures, the large-polaron mobility can be written as [38]

$$\mu(T) \propto eL^2(T_L/T)^4, \tag{7}$$

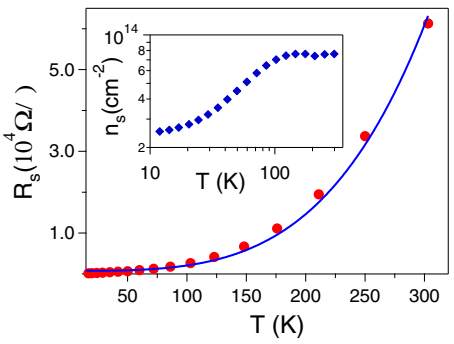

FIG. 6. Sheet resistance R (dots) of the q-2DES under amorphous LAO, measured on sample B and fit (solid line) to the large-polaron model of Eq. (8). Inset: surface charge density n_s vs temperature as determined by Hall measurements.

where L is the polaron dimension and $T_L = \hbar c_s/(k_B L)$, with c_s being the velocity of sound in the solid. The sheet resistance R measured in sample B and reported in Fig. 6 can then be fit by

$$R(T) \propto [n_s(T)e\mu(T)]^{-1} \propto T^4 \exp(\Delta/2k_B T). \tag{8}$$

The excellent fit to Eq. (8) shown by the solid line in Fig. 6 provides, for the polaronic charges, a binding energy $\Delta \simeq 190k_B$. Therefore, with such a weak activation energy, the photoexcitation of the charges in the midinfrared will provide a T-independent n_s^{IR}, which should be compared with the n_s^{dc} measured at saturation above 100 K (see the inset of Fig. 6). In Fig. 6 this value is still lower than that in Table II by a factor of 3, also possibly because it was taken after the Berreman experiments. Some sample degradation might be expected due to the thermal cycles needed for the infrared measurements and to the time that has elapsed.

In Table II we do not report μ^{IR} for sample B because, following Ref. [29], only the width of the Berreman dip does not provide a meaningful estimate of Γ_D, the carrier relaxation rate. Moreover, when fitting only the dip, n^{IR} and the q-2DES thickness d are correlated, as shown in Fig. 3 of the SM. The large errors reported for these quantities in Table II were obtained by building up at any T a distribution of all their values, which allowed us to obtain several fits to the $\Delta\Psi$ of sample B which all have the same accuracy. The central values and standard deviations of those distributions are reported in Table I (for d) and Table II (for n^{IR} and, consequently, n_s^{IR}). Table II also displays the dc mobility extracted from data in Fig. 6 and in Fig. 1 of the SM [28]. One may notice that μ^{dc} is surprisingly high at low temperature, even better than in our crystalline sample (sample A).

The lack of a Berreman peak close to the dip at 868 cm^{-1} in sample B can be attributed to an insufficient signal-to-noise ratio where the reflectivity becomes too low or to the charge-density profile within the q-2DES [8], which smears out the feature through a distribution of plasma frequencies. We can also tentatively explain that absence as follows. According to numerical simulations of the BE reported in the literature [8,20], while the dip frequency remains fixed, the Berreman peak shifts rapidly to higher frequencies as ω_p increases. This is confirmed by Fig. 7, where the energy loss function $\Xi(\omega) = \mathrm{Im}[-1/\tilde{\epsilon}(\omega)]$ is plotted for both samples A and B as extrapolated from $\tilde{\epsilon}_1$ in Eq. (6). We recall that the BE resonance, being a longitudinal spectral feature, is associated

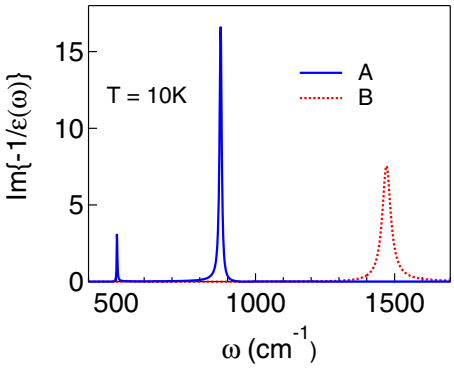

FIG. 7. Energy-loss function calculated for both crystalline (sample A) and amorphous LAO (sample B) from the dielectric function which fits to the data at 10 K. The peaks correspond to the Berreman resonances at ω_{Ber}. Those at 502 cm^{-1} (sample A) and 1479 cm^{-1} (sample B) give rise to very weak features in the ellipsometric angle Ψ, not reported in the previous figures.

with a peak in $\Xi(\omega)$ [22]. As one can see, while for sample A the peak corresponds exactly to that in $\Delta\Psi$ of Fig. 2, that of sample B should be displaced (in an ideal q-2DES system) to 1480 cm^{-1}, far away from the highest LO phonon of STO. Therein, however, Ψ does not show any reproducible Berreman peak. One can tentatively assume that the peak is not observed because R_p/R_s is low and the peak at ω_{Ber} is broadened a great deal by the disorder induced in the interface by amorphous LAO. One may also notice that a weaker peak in $\Xi(\omega)$ is predicted in the region of the LO2 phonon of sample A, shifted by 23 cm^{-1} from ω_{L2}. However this feature, like the one at 1480 cm^{-1}, has not been observed in the present experiment. In general, the weakness of the BE resonances in this q-2DES is not surprising if one recalls that, for a thin film, the optimum thickness to observe the BE is given by [22]

$$d_{\rm opt} = (\lambda/2\pi)(\cos\theta/\sin^2\theta)\Xi_{\rm max}. \quad (9)$$

Inserting in Eq. (9) our experimental values, one finds $d_{\rm opt}$ = 37 nm for the q-2DES of crystalline LAO and $d_{\rm opt}$ = 70 nm for that of amorphous LAO. In both our samples (see Table II), the thickness d of the q-2DES is smaller than $d_{\rm opt}$ by an order of magnitude.

IV. CONCLUSION

In conclusion, we have used grazing-angle infrared spectroscopy and the Berreman effect to investigate the electrodynamics of the quasi-two-dimensional electron system (q-2DES) which forms spontaneously at the $LaAlO_3/SrTiO_3$ interface both when the LAO film is crystalline (sample A) and when it is amorphous (sample B). In the latter case we have not observed the complete BE shape, and we have tentatively explained this result by a hardening and broadening of the Berreman peak caused by the unexpectedly high carrier density n_s in sample B and by disorder at the interface, respectively. Nevertheless, the BE has been shown once again to be a powerful tool to detect the electrodynamic response of ultrathin conducting films in the no-contact mode. With accurate fits to the BE resonances of both samples we have found that the thickness of the q-2DES is 4 ± 1 nm under crystalline LAO and 7 ± 2 nm under amorphous LAO. Resistance and Hall measurements in sample B confirmed its high carrier density, even if the room temperature value of n_s^{dc} is smaller than the previously measured n_s^{IR} by about a factor of 3. Moreover, unlike n_s^{IR}, n_s^{dc} decreases below 100 K, as also reported in Ref. [8] for crystalline LAO, indicating that part of the charges originate from a shallow localized state, which possibly can be described as a large polaron, that, having an ionization energy of about 190 K, cannot affect the midinfrared spectra. Even if the q-2DES charge density in LAO/STO is known to strongly depend on the film growth conditions, it remains that it can assume quite high values also in the presence of amorphous LAO, where the dc carrier mobility is also surprisingly high. These results may be of interest for the present research effort aimed at better understanding the properties of the LAO/STO interface and at exploiting them in the different applications that are being proposed for this intriguing system.

ACKNOWLEDGMENTS

We wish to thank A. Dubroka for illuminating discussions. This work has been partially supported by the Italian Ministry of University and Research through the PRIN project OXIDE and by the European Commission CALIPSO Programme (HZBPHOTONS-CALIPSO-140) for access to the synchrotron facilities. We also acknowledge SOLEIL for provision of beamtime under the Proposal 20160221 and we thank for assistance all personnel of the AILES beamline.

[1] W. T. Sommer, Phys. Rev. Lett. **12**, 271 (1964).
[2] A. K. Geim, Science **324**, 1530 (2009).
[3] M. Z. Hasan and C. L. Kane, Rev. Mod. Phys. **82**, 3045 (2010).
[4] J. E. Moore, Nature (London) **464**, 194 (2010).
[5] A. Ohtomo, D. A. Muller, J. L. Grazul, and H. Y. Hwang, Nature (London) **419**, 378 (2002); A. Ohtomo and H. Y. Hwang, *ibid.* **427**, 423 (2004).
[6] J. Mannhart and D. G. Schlom, Science **327**, 1607 (2010).
[7] M. Basletic, J.-L. Maurice, C. Carrétéro, G. Herranz, O. Copie, M. Bibes, E. Jacquet, K. Bouzehouane, S. Fusil, and A. Barthélémy, Nat. Mater. **7**, 621 (2008).
[8] A. Dubroka, M. Rössle, K. W. Kim, V. K. Malik, L. Schultz, S. Thiel, C. W. Schneider, J. Mannhart, G. Herranz, O. Copie, M. Bibes, A. Barthélémy, and C. Bernhard, Phys. Rev. Lett. **104**, 156807 (2010).
[9] A. Brinkman, M. Huijben, M. Van Zalk, J. Huijben, U. Zeitler, J. C. Maan, W. G. Van der Wiel, G. Rijnders, D. H. A. Blank, and H. Hilgenkamp, Nat. Mater. **6**, 493 (2007).
[10] N. Reyren, S. Thiel, A. D. Caviglia, L. Fitting Kourkoutis, G. Hammerl, C. Richter, C. W. Schneider, T. Kopp, A.-S. Rüetschi, D. Jaccard, M. Gabay, D. A. Muller, J.-M. Triscone, and J. Mannhart, Science **317**, 1196 (2007).

[11] L. Li, C. Richter, J. Mannhart, and R. C. Ashoori, Nat. Phys. **7**, 762 (2011).
[12] J. A. Bert, B. Kalisky, C. Bell, M. Kim, Y. Hikita, H. Y. Hwang, and K. A. Moler, Nat. Phys. **7**, 767 (2011).
[13] E. Di Gennaro, U. Scotti di Uccio, C. Aruta, C. Cantoni, A. Gadaleta, A. R. Lupini, D. Maccariello, D. Marré, I. Pallecchi, D. Paparo, P. Perna, M. Riaz, and F. Miletto Granozio, Adv. Opt. Mater. **1**, 834 (2013).
[14] G. M. De Luca, R. Di Capua, E. Di Gennaro, F. M. Granozio, D. Stornaiuolo, M. Salluzzo, A. Gadaleta, I. Pallecchi, D. Marré, C. Piamonteze, M. Radovic, Z. Ristic, and S. Rusponi, Phys. Rev. B **89**, 224413 (2014).
[15] A. D. Caviglia, S. Gariglio, C. Cancellieri, B. Sacepe, A. Fete, N. Reyren, M. Gabay, A. F. Morpurgo, and J. M. Triscone, Phys. Rev. Lett. **105**, 236802 (2010).
[16] P. R. Willmott, S. A. Pauli, R. Herger, C. M. Schleputz, D. Martoccia, B. D. Patterson, B. Delley, R. Clarke, D. Kumah, C. Cionca, and Y. Yacoby, Phys. Rev. Lett. **99**, 155502 (2007).
[17] A. Kalabukhov, R. Gunnarsson, J. Borjesson, E. Olsson, T. Claeson, and D. Winkler, Phys. Rev. B **75**, 121404(R) (2007).
[18] Y. Chen, N. Pryds, J. E. Kleibeuker, G. Koster, J. Sun, E. Stamate, B. Shen, G. Rijnders, and S. Linderoth, Nano Lett. **11**, 3774 (2011).
[19] R. Pentcheva and W. E. Pickett, Phys. Rev. B **74**, 035112 (2006).
[20] M. Yazdi-Rizi, P. Marsik, B. P. P. Mallett, K. Sen, A. Cerreta, A. Dubroka, M. Scigaj, F. Sánchez, G. Herranz, and C. Bernhard, Phys. Rev. B **95**, 195107 (2017).
[21] D. W. Berreman, Phys Rev. **130**, 2193 (1963).
[22] B. Harbecke, B. Heinz, and P. Grosse, Appl. Phys. A **38**, 263 (1985).
[23] M. Born and E. Wolf, *Principles of Optics* (Pergamon, Oxford, 1959).
[24] A. Nucara, M. Ortolani, L. Baldassarre, W. S. Mohamed, U. Schade, P. P. Aurino, A. Kalaboukhov, D. Winkler, A. Khare, F. Miletto Granozio, and P. Calvani, Phys. Rev. B **93**, 224103 (2016).
[25] P. P. Aurino, A. Kalaboukhov, N. Tuzla, E. Olsson, T. Claeson, and D. Winkler, Appl. Phys. Lett. **102**, 201610 (2013).
[26] P. Roy, J.-B. Brubach, P. Calvani, G. De Marzi, A. Filabozzi, A. Gerschel, P. Giura, S. Lupi, O. Marcouillé, A. Mermet, A. Nucara, A. Paolone, and M. Vervloet, Nucl. Instrum. Methods Phys. Res., Sect. A **467**, 426 (2001).
[27] V. K. Guduru, A. Granados del Aguila, S. Wenderich, M. K. Kruize, A. McCollam, P. C. M. Christianen, U. Zeitler, A. Brinkman, G. Rijnders, H. Hilgenkamp, and J. C. Maan, Appl. Phys. Lett. **102**, 051604 (2013).
[28] See Supplemental Material at http://link.aps.org/supplemental/10.1103/PhysRevB.97.155126 for the raw reflectivity data of the three samples, and for the anticorrelation between the plasma frequency and the q-2DES thickness in the Berreman fits.
[29] S. Y. Park and A. J. Millis, Phys. Rev. B **87**, 205145 (2013).
[30] P. Calvani, M. Capizzi, F. Donato, P. Dore, S. Lupi, P. Maselli, and C. P. Varsamis, Phys. C (Amsterdam, Neth.) **181**, 289 (1991).
[31] M. Dressel and G. Grüner, *Electrodynamics of Solids* (Cambridge University Press, Cambridge, 2002).
[32] F. Gervais, J.-L. Servoin, A. Baratoff, J. G. Bednorz, and G. Binnig, Phys. Rev. B. **47**, 8187 (1993).
[33] M. Yazdi-Rizi, P. Marsik, B. P. P. Mallett, A. Dubroka, D. V. Christensen, Y. Z. Chen, N. Pryds, and C. Bernhard, Europhys. Lett. **113**, 47005 (2016).
[34] P. Calvani, Riv. Nuovo Cimento **24**, 1 (2001).
[35] L. Forro, O. Chauvet, D. Emin, L. Zuppiroli, H. Berger, and F. Lévy, J. Appl. Phys. **75**, 633 (1994).
[36] J. T. Devreese and A. S. Alexandrov, Rep. Prog. Phys. **72**, 066501 (2009).
[37] M. Ziese and C. Srinitiwarawong, Phys. Rev. B. **58**, 11519 (1998).
[38] D. Emin, *Polarons* (Cambridge University Press, Cambridge, 2013), p. 93.